

Inertial effects in droplet spreading: a comparison between diffuse-interface and level-set simulations

HANG DING AND PETER D. M. SPELT

Department of Chemical Engineering, Imperial College London, SW7 2AZ, UK

(Received 24 August 2006 and in revised form 16 January 2007)

Axisymmetric droplet spreading is investigated numerically at relatively large rates of spreading, such that inertial effects become important. Results from two numerical methods that use different means to alleviate the stress singularity at moving contact lines (a diffuse interface, and a slip-length-based level-set method) are shown to agree well. An initial inertial regime is observed to yield to a regime associated with Tanner's law at later times. The spreading rate oscillates during the changeover between these regimes. This becomes more significant for a fixed (effective) slip length when decreasing the value of an Ohnesorge number. The initial, inertia-dominated regime is characterized by a rapidly extending region affected by the spreading, giving the appearance of a capillary wave travelling from the contact line. The oscillatory behaviour is associated with the rapid collapse that follows the point at which this region extends to the entire droplet. Results are presented for the apparent contact angle as a function of dimensionless spreading rate for various values of Ohnesorge number, slip length and initial conditions. The results indicate that there is no such universal relation when inertial effects are important.

1. Introduction

We consider here the spreading of a droplet on a wall, at rates of spreading such that the instantaneous value of the Reynolds number $Re = \rho RU/\mu$ is significant, where R is the radius of the contact line, U is the contact-line speed, and ρ and μ are the density and dynamic viscosity of the droplet. Effects of inertia in droplet spreading have been widely studied, but usually in the context of droplet impact on a dry wall, in which case the spreading is dominated by kinetic effects resulting directly from the impact (for a recent review see Yarin 2006). We investigate here the inertial effects resulting from the spreading motion itself. Numerical methods are used for this purpose, supplementing earlier experimental and theoretical work, that we briefly review here.

An inertial spreading regime has been identified experimentally by Biance, Clanet & Queré (2004), where a sessile droplet was brought carefully in contact with a plate, on which the droplet spread. The radius of the wetted area approximately followed $R \sim t^{1/2}$ at early times, with a sudden transition to the well-documented Tanner law $R \sim t^{1/10}$ (Tanner 1979) at later times. Biance *et al.* (2004) presented a scaling argument, based on a force balance for the part of the droplet involved in the spreading process, which resulted in convincing agreement with the data. The scaling argument is valid for small times, such that R is much smaller than the droplet

radius. A main step in this force balance is the notion that the fraction of the droplet involved in the spreading process depends on time.

Measurements of the interface shape in the contact-line region have been performed by Stoev, Ramé & Garoff (1999), for a range of Re and capillary numbers, $Ca = \mu U / \sigma$, where σ is the coefficient of surface tension. Although results were not obtained for droplet spreading, but for a solid entering a pool, their results indicate that, on a macroscopic scale, the apparent contact angle is decreased by inertial effects.

The observations by Stoev *et al.* (1999) substantiate an earlier analysis by Cox (1998), to some extent, wherein it is assumed that $1/\lambda \gg Re \gg 1$, where λ is (in the present notation) the slip length made dimensionless with the initial drop radius. (A second analysis by Cox (1998) for $\lambda Re \gg 1$ is beyond the scope of this paper.) The result obtained by Cox indicates that apparent contact angles decrease at larger values of Re , as observed experimentally, but showed no quantitative agreement with measurements.

The spreading of thin droplets with significant inertia was investigated in detail by Hocking & Davis (2002), who used a lubrication approach (with a slip condition). They showed that a simple relation between apparent contact angle and U does not exist at sufficiently large values of Re . At a fixed value of λ , there exists a critical value of Re beyond which the approach to the static droplet shape becomes oscillatory. This critical value of Re decreases for increasing values of λ .

In this paper we use numerical simulations to study inertial effects in axisymmetric droplet spreading. Most related previous numerical studies have focused on the impact of a drop on a wall; an exception is the early study by Renardy, Renardy & Li (2001), who presented results for a single test case of spreading (of a planar two-dimensional droplet) for their VOF scheme.

Practical restrictions on the computations limit this study in two ways. First, the inertial effects investigated are primarily on the scale of the entire droplet. Hence Re reaches values up to $O(10^2)$, which will be seen in §3 to have substantial effects on the spreading process, but Reynolds numbers based on the dimensions of the contact-line region, λRe or $\lambda U / Oh$ using the present time scaling in §3.2, are up to $O(1)$. A study of large inertial effects in the contact-line region (as investigated previously by Cox 1998, using analysis) is therefore not attempted here.

The second limitation of this study is that the numerical methods adopted here cannot be used to resolve the flow accurately on a length scale smaller than that corresponding to $\lambda = O(10^{-2})$. This falls well short of realistic conditions for millimetric droplets, which would demand $\lambda = O(10^{-4})$ at most (Marsh, Garoff & Dussan V. 1993; Eggers & Stone 2004). Nevertheless, our previous work shows that results for the range of values of λ achieved here capture the main trends known for much smaller values of λ . Numerical results for two-dimensional planar flows obtained from an earlier version of a code used here (Spelt 2005) appear to converge to a lubrication theory for thin droplets at values of λ similar to those used here. A further comparison with lubrication theory is performed in §2, and the effect of the slip length is investigated in §3.

Several formulations are available to alleviate the stress singularity at the moving contact line (e.g. Huh & Scriven 1971; Dussan V. 1979). We use here two different methods, implemented separately: a slip-length-based level-set (LS) method (Spelt 2005), and a diffuse interface (DI) method (Jacqmin 1999, 2000). Alternative methods include a precursor film (de Gennes 1985) and surface-tension relaxation (Shikhmurzaev 1997). A comparison between the two methods establishes the sensitivity of the results to the manner in which the stress singularity is alleviated, and allows translation of results between these two methods.

2. Numerical method

The DI method used here generally follows Jacqmin (1999, 2000), except that the volume fraction of the droplet fluid C is chosen as the order parameter, which is governed by the convective Cahn–Hilliard equation:

$$\frac{\partial C}{\partial t} + \mathbf{u} \cdot \nabla C = \nabla \cdot (M \nabla \phi), \quad (2.1)$$

where M is the mobility, $\phi = 6\sqrt{2}\sigma(\zeta^{-1}\Psi'(C) - \zeta\Delta C)$ is the chemical potential, $\Psi(C) = \frac{1}{4}C^2(1-C)^2$ is the bulk energy density, σ is the coefficient of surface tension and ζ is a measure of the thickness of the diffuse interface. The diffuse interface is a narrow miscible gap of $O(\zeta)$ thickness, separating the two fluids. The diffusion term in (2.1) originates from thermodynamics, and provides a mechanism to maintain the regularity of the diffuse interface. A prescribed contact angle value θ_w results in the following boundary condition for the volume fraction:

$$\tan\left(\frac{\pi}{2} - \theta_w\right) = \frac{-\mathbf{n} \cdot \nabla C}{|\nabla C - (\mathbf{n} \cdot \nabla C)\mathbf{n}|}, \quad (2.2)$$

where \mathbf{n} is the unit outward normal defined at the wall. The diffusive flux through the boundary is set to zero, $\mathbf{n} \cdot \nabla \phi = 0$, irrespective of the contact angle imposed. Finally, the surface tension force is computed by $\mathbf{f}_{st} = \phi \nabla C$ (Jacqmin 1999).

The equations of motion were solved on a MAC grid. The code has been validated for the axisymmetric breakup of a rising bubble at very large density contrast (1:1000), as well as for the nonlinear evolution of a Rayleigh–Taylor instability. Typical loss in the total mass of the droplet is of order of ‘machine accuracy’. In the DI method, the no-slip condition is used; the motion of contact lines is due to the diffusive flow rate that occurs in the diffuse interface region. The results of the DI method at a given value of ζ can be approximated by lubrication theory if an appropriate value of the slip length is used. The comparison indicates that the thickness of the diffuse interface is related to an ‘effective’ slip length. At the end of this section we describe how we determine the effective slip length by fitting our results to the prediction of the lubrication theory.

The LS method used here is essentially that of Spelt (2005, 2006), where details of convergence rates and mass conservation can be found. The only modification is the change from two-dimensional Cartesian to cylindrical coordinates. The contact-line speed is obtained as in the previous work, i.e. it is averaged over the time for the contact line to move through several grid cells (Spelt 2005). The LS code uses the slip condition at the wall, $v = \lambda \mathbf{n} \cdot \nabla v$, where v denotes the velocity component of fluid parallel to the wall.

The two numerical methods are used here to study axisymmetric droplet spreading. We isolate the inertial effects caused by the spreading process, as opposed to e.g. those arising directly from the impact of a droplet on a wall, by choosing the initial drop shape as corresponding to a circular-cap droplet, which would have a contact angle θ_0 (typically $\theta_0 = \pi/3$ or $2\pi/3$) were it not that a different microscale contact angle θ_w is prescribed (typically $\theta_w = \pi/18$). The droplet therefore spreads to a static shape corresponding to the microscale contact angle, θ_w . The instantaneous capillary and Reynolds numbers both depend on the contact-line speed. In order to distinguish between different simulations, we shall present results for constant values of the Ohnesorge number

$$Oh = \sqrt{Ca/Re} = \frac{\mu}{\sqrt{\rho\sigma R_0}}, \quad (2.3)$$

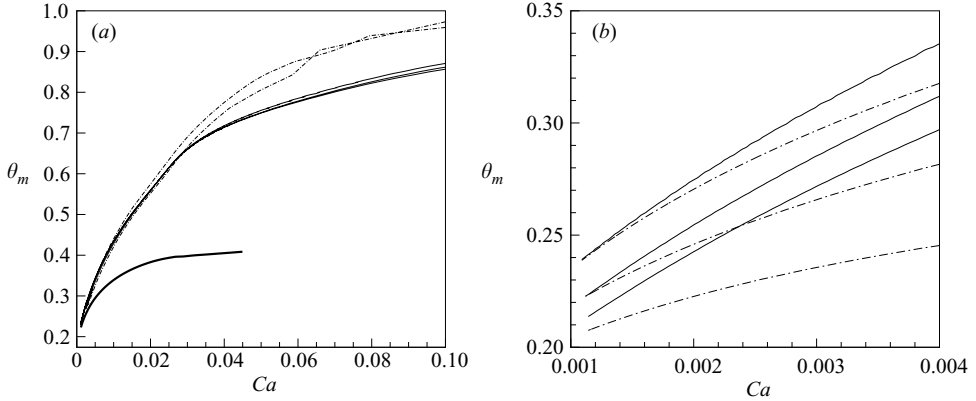


FIGURE 1. (a) Convergence study and comparison with theory for the apparent contact angle as a function of Ca at $Oh=0.141$. Solid lines are DI, dash-dotted lines are LS results; the grid spacing for DI is (from top to bottom) $\Delta r = 1/150, 1/200, 1/250$ (the last two virtually overlap); for LS, $\Delta r = 1/128, 1/256$ (from bottom to top). The thick solid line is (2.4) for $\lambda=0.01$. (b) Comparison between (2.4) (dash-dotted lines) and the DI method results (solid lines) with $\zeta = 0.00375, 0.005, 0.00625$ and $\Delta r = 1/200$ (from top to bottom).

which only depends on fluid parameters and the characteristic length scale used in this paper, the initial radius of the droplet R_0 .

Results for different values of the grid spacing Δr ($= \Delta z$ in both methods, where the z -axis is the axis of symmetry) are presented in figure 1(a), as the apparent contact angle θ_m , defined as the maximum angle between the interface and the horizontal within a distance of $0.2R_0$ from the contact line, versus the dimensionless instantaneous velocity of the contact line (i.e. Ca), with time as the parameter along the curve. The results from the DI method are for a constant thickness of diffuse interface (corresponding to dimensionless $\zeta = 0.005$). These agree quite well with the results obtained from the LS method for a dimensionless slip length of $\lambda = 0.01$, for Ca up to about 0.03, as well as with the lubrication theory for this slip length at very low Ca , despite the relatively large value of the slip length. The sensitivity of the LS results to the grid spacing are similar as those reported in Spelt (2005). The comparison worsens at larger values of Ca , however. Although it is difficult to speculate about the origin of this, note that the initial radius of curvature of the interface near the contact line is very small, possibly smaller than the thickness of the diffuse interface (usually the thickness between $C = 0.05$ and $C = 0.95$ is around 4ζ), and this may lead to some differences with results from the LS method at large values of Ca .

Villanueva & Amberg's (2006) concluded that the apparent contact angle is 'fairly independent of interface width' in their DI simulations. We investigate this in more detail in figure 1(b), where results from the DI method are compared with lubrication theory (based on a slip condition) for different values of the thickness of the diffuse interface. The apparent contact angle predicted by the lubrication theory yields (Hocking 1983)

$$\theta_m^3 = \theta_w^3 + 9Ca^{cl} \ln(R\theta_w / (6e\lambda)), \quad (2.4)$$

where $Ca^{cl} \equiv \mu_1 U / \sigma$ and $R(t)$ is the instantaneous dimensionless drop radius.

Jacqmin (2000) showed that, when assuming that $\zeta / \sqrt{\mu M} \rightarrow 0$, the effective slip length caused by the diffuse interface is proportional to $\sqrt{\mu M}$. However, in our

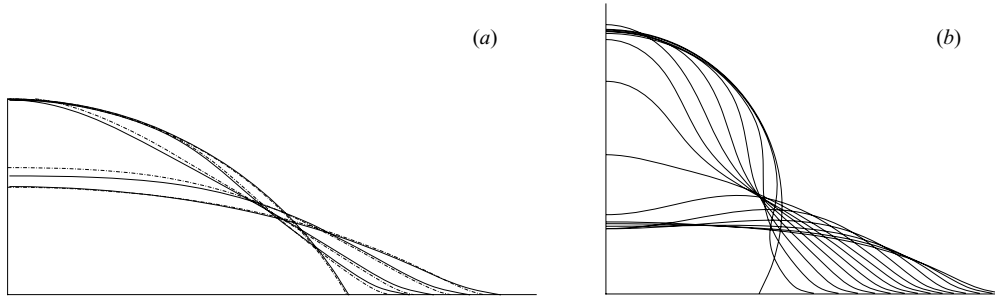


FIGURE 2. Snapshots of droplet interface shapes during spreading for initial values of θ_m equal to (a) $\pi/3$ and (b) $2\pi/3$. The droplet volume is the same in both cases; $Oh = 0.0354$. Solid lines represent results from the DI method, dash-dotted lines are from the LS method ((a) only). In (a), $t = 0, 0.113, 0.226, 0.452, 0.679$; in (b), the time interval is 0.057.

studies $\zeta/\sqrt{\mu M}$ is $O(1)$, and we find that the effective dimensionless slip length λ_{di} is not sensitive to the viscosity, but that we can write, to a reasonable approximation, $\lambda_{di} = \alpha\zeta$, where α is approximately constant. The coefficient α can be determined by approximating the numerical results by (2.4) with an appropriate slip length in the small- Ca regime. In figure 1(b), the numerical result with $\zeta = 0.005$ is first fitted to that predicted by the lubrication theory, giving a dimensionless effective slip length $\lambda_{di} = 0.009$, then the constant obtained ($\alpha = 1.8$) is used in the lubrication theory approximations of larger interfacial characteristic lengths. A deviation is seen only for the largest value of ζ , but one would expect the comparison to get worse in such cases, especially because of the limitations in the validity of the lubrication theory. In any case, in figure 1(b) the slope of the numerical and analytical results become quite close at the smallest value of ζ simulated here. We conclude that $\alpha = 1.8 \pm 0.2$. We compare results from the two computational methods in the sections below by setting $\alpha = 2$ (as is also used in figure 1a). As will be seen in figure 6, the methods agree quite well for a range of values of Oh . Close inspection of Villanueva & Amberg's (2006), results indicates that the contact-line speed decreases with the thickness of the diffuse interface, as observed here.

3. Results

3.1. Interface shapes

Some main features of the spreading process at moderate values of Re can be observed in figure 2, where sequences of drop shapes are shown for $\theta_0 = \pi/3$ and $2\pi/3$ (the experimental case of $\theta_0 = \pi$ being beyond the reach of the present simulations), and $Oh = 0.0354$. The interface resulting from the DI method corresponds to the $C = 0.5$ contour. Several observations can be made from these results. First, the results of the two numerical methods agree reasonably well. The LS method predicts spreading rates that are lower than those obtained from the DI method, but there appear to be no other differences. Secondly, the dynamical behaviour at short times is markedly different from that at later times in the spreading process. The late-time behaviour is the well-documented process of the uniform decrease in droplet height (near the droplet centre) during spreading. At early times though, the drop height only decreases in a small region close to the contact line, whereas the drop height at the axis of symmetry remains almost stationary. This spreading-affected region increases with time, giving the appearance of a capillary wave with the wavefront propagating

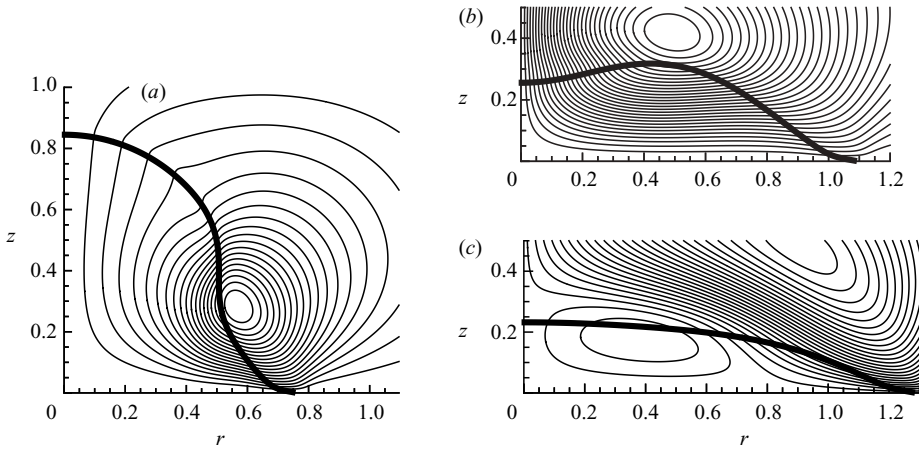


FIGURE 3. Instantaneous streamlines obtained from the DI method for the case shown in figure 2(b) at times $t = 0.057$ to 0.868 during the initial (a) $t = 0.057$ and oscillatory regime (b) $t = 0.509$ and (c) $t = 0.848$. The spacing between the values of streamline contours is 0.01. The thick line corresponds to the contour $C = 0.5$, indicative of the interface location.

from the contact line to the top of the droplet. This finding is very similar to the experimental observations of Biance *et al.* (2004).

Figures 2 and 3 provide further details. In figure 3, instantaneous streamlines show how at short times, strong flow occurs approximately along the outwards-directed normal vector at the drop surface, in a region close to the contact line. When the resulting ‘wavefront’ reaches the top of the droplet, and when the droplet centre has collapsed to a temporary minimum, some oscillations in the drop height occur. Because of the set-up used in Biance *et al.* (2004), this stage has not been observed experimentally. In figure 3(b) the collapse of the drop centre is further seen to affect the flow inside the droplet. It pumps the flow outward from the centre and consequently speeds up the spreading of the droplet. Figure 3(c) shows that at this stage of spreading the drop height decreases only over a small region. This was not observed in figure 3(a) and we will return to this in §3.3.

3.2. Time scaling

The features of dynamical behaviour at the initial stage of droplet spreading are observed on an inertial/capillary time scale $T = \sqrt{\rho R_0^3 / \sigma}$. This time scale represents the natural response time if the droplet is taken as a spring with the coefficient of surface tension as the stiffness (as pointed out previously by Biance *et al.* 2004). Figure 4 shows the dimensionless spreading rate (essentially the Reynolds number based on the dimensionless slip length) as a function of time made dimensionless with T for various values of Oh . It is seen that the oscillation in spreading rate, which indicates the return of the capillary wave to the contact line, occurs synchronically in the three cases, thereby supporting the time scaling used here.

3.3. Rate of spreading

The spreading rate is shown as a function of time in figure 5 for various values of Oh (Oh was varied by changing the value of the viscosity). Two familiar regimes can be identified. At $Oh = 0.283$ (the largest value simulated here), the spreading velocity approaches a $t^{-0.9}$ regime at long times, consistent with Tanner’s law (Tanner 1979). At $Oh = 0.0141$ and 0.00707 , the smallest considered here, the spreading rate

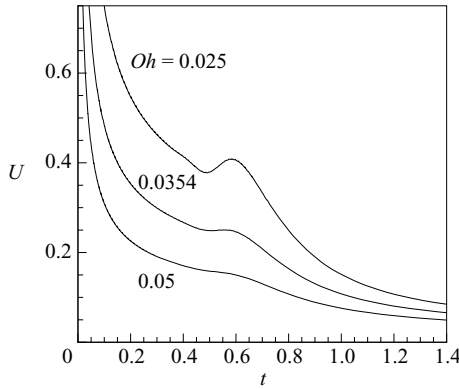


FIGURE 4. Effect of Oh on the dependence of the instantaneous dimensionless spreading rate on the dimensionless time (as explained in the text). DI method for $\lambda=0.01$ and different values of Oh obtained by varying the surface tension coefficient.

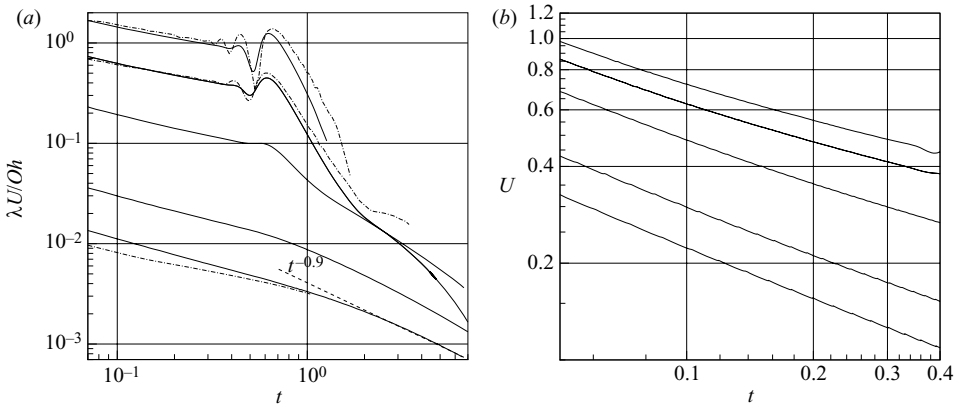


FIGURE 5. Instantaneous dimensionless spreading rate versus time, for various values of Oh , where the initial value of $\theta_m = \pi/3$, $\lambda = 0.01$ and $Oh = 0.283, 0.141, 0.0354, 0.0141,$ and 0.00707 (from bottom to top). (a) Spreading rate, where the solid and dash-dotted lines indicate results from the DI and LS methods, respectively; (b) detail of the DI results for U in (a).

is much larger, and the droplet is approaching its static shape rapidly, resulting in an exponential regime in the spreading rate within the time span shown. Assuming that $\theta - \theta_w \ll \theta_w$, (2.4) can be integrated to give (see also Hocking 1983)

$$U \sim \exp\left[-\theta_w^3 t / (R_\infty Oh \ln [R_\infty \theta_w / (6e\lambda)])\right], \tag{3.1}$$

where R_∞ is the dimensionless equilibrium radius of the contact line. For the present simulations with $Oh = 0.0141$, the exponent is -0.38 ; the simulations give a value of -0.44 . At early times, the spreading rate exhibits a regime that is approximately a power-law. The results obtained from the DI method can be fitted reasonably well by $U \sim t^{-0.45}$ (apparently tailing off to $t^{-0.4}$ at intermediate times). The results from the LS method show a somewhat different exponent, $U \sim t^{-0.35}$. These findings compare surprisingly well with the experimental results of Biance *et al.* (2004) that correspond to a spreading velocity $U \sim t^{-0.48 \pm 0.05}$ (their theoretical analysis showed $U \sim t^{-0.5}$). As shown in figure 5(b), the proportionality factor in these relations is weakly dependent

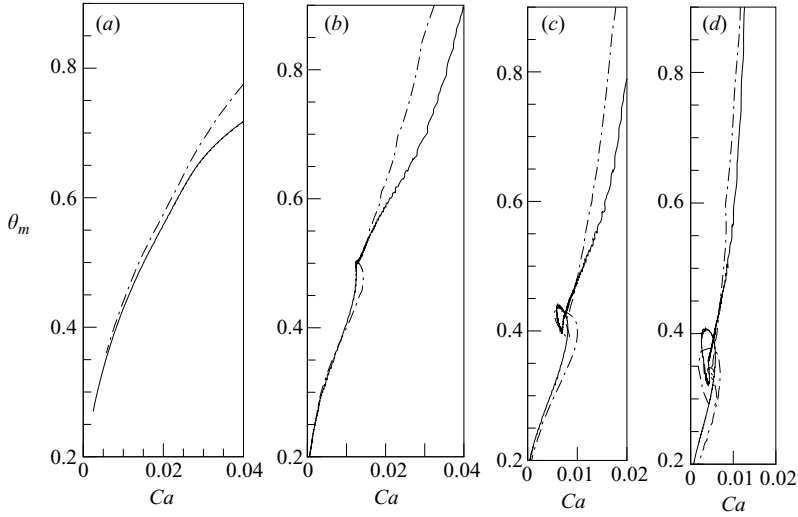


FIGURE 6. Apparent contact angle as a function of capillary number for (a) $Oh=0.141$, (b) 0.0354 , (c) 0.0141 , and (d) 0.00707 . The solid and dash-dotted lines indicate results from the DI and LS methods, respectively.

on Oh but appears to converge with decreasing Oh . Biance *et al.* explained this regime to result from the curvature-driven surface-tension force being only experienced by a fraction of the droplet, which increases in time. The argument does not account for viscous effects. The comparison is therefore tentative; the Reynolds number in the experiments was $O(10^3)$, well above the values in the present simulations.

The transition between the early and late regime at sufficiently small values of Oh is seen to be accompanied by oscillations in the spreading rate. By comparison with figure 2(a), it is seen that this oscillatory spreading occurs exclusively during the collapse of the centre of the droplet, following the arrival of the wave at the top of the drop. Careful observation of the interface shape in figure 2(a) shows that the top of the drop bulges out in the region where the interface tangent is the largest, delaying the decrease in θ_m with increasing time. This effect is of course much more pronounced in figures 2(b) and 3. In particular, the stage shown in figure 3(b) corresponds to a local minimum in θ_m . It is tempting to relate these findings to the analytical work by Hocking & Davis (2002), but the oscillations in the spreading rate discovered there relate to the final, exponential approach to the static shape. The Reynolds numbers during the exponential stage in the present simulations are significantly below the critical values of Hocking & Davis (2002), and no oscillations in that regime are observed here.

3.4. Apparent contact angle

The maximum tangent of the interface is plotted in figure 6 as a function of the instantaneous value of Ca , for various values of Oh . The thickness of the diffuse interface in the DI method, and the dimensionless slip length in the LS method were kept constant at $\zeta=0.005$ and $\lambda=0.01$, respectively. At small Oh , a sudden transition is observed, corresponding to the change in spreading regime discussed in §3.3. Clearly, θ_m is not a single-valued function of Ca . In fact, it is clear from figure 7(a) that the relation between apparent contact angle and contact-line speed is

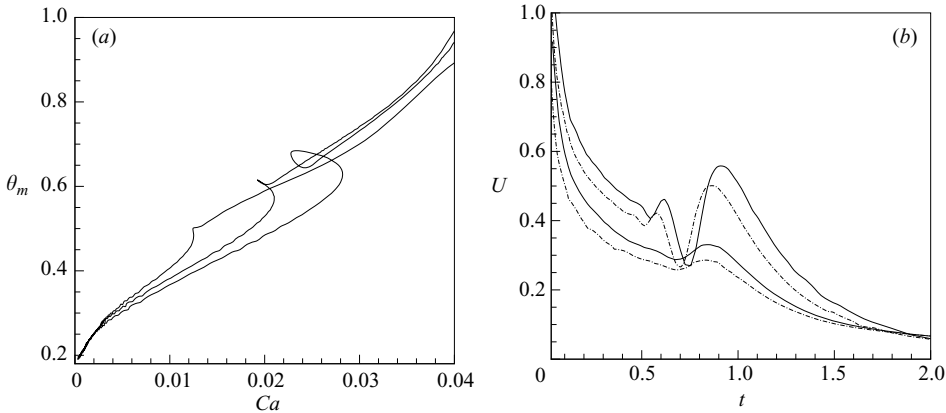


FIGURE 7. (a) Apparent contact angle as a function of capillary number for initial apparent angles of $\pi/3$, $\pi/2$ and $2\pi/3$ (from left to right). DI method for $Oh=0.0354$, $\zeta=0.005$. (b) Effect of dimensionless slip length on spreading rate as a function of time. The dash-dotted and solid lines are for $\lambda=0.01$ and 0.02 , respectively. The upper two lines are for $Oh=0.0141$, the two lower lines for $Oh=0.0354$. Results are for the LS method.

sensitive to the initial conditions of the flow. Only at rather small values of Ca do the results approach each other.

The results at $Ca < 0.01$ in figure 6 show that a decrease in Oh leads to a slightly lower value of θ_m , which supports the findings of Cox (1998) and Stoev *et al.* (1999). The sensitivity to inertial effects is however completely dominated by the converse increase in θ_m at larger Ca , i.e. during the initial spreading regime. In the regime of very large Ca , corresponding to the very beginning of the simulation, the difference in the apparent contact angle between the two computational methods can be attributed to their different ways of resolving the initial curvature singularity at the contact line.

3.5. Effect of slip length

A main effect of reducing the (effective) slip length, thereby approaching experimental conditions, is a reduction in contact-line speed. Trends such as the oscillatory regime should therefore be observed at lower values of λ by choosing a smaller value of Oh . This is confirmed in figure 7(b), where we plot U as a function of time at two values of λ , each at two values of Oh . The oscillations in the spreading rate reduce when reducing λ , but this can be overwhelmed by the sensitivity to Oh .

4. Conclusions

Results from LS and DI methods, which agree well, show that inertial effects cause droplet spreading to be non-monotonic, and that this is strongly dependent on initial conditions, Oh and the slip length. The simulations support the experimental findings of Bianco *et al.* (2004), but provide further detail, especially regarding the transition from an inertia-dominated to a viscous regime, which is seen to be non-monotonic. The non-monotonic spreading is associated with the increasing region in the droplet affected by spreading, giving the appearance of a capillary wave that travels from the contact line to the top of the droplet, leading to a rapid collapse of the droplet centre. The apparent contact angle is only independent of initial conditions at low values of Ca . Attempts to collapse data for different values of the slip length (as in Spelt 2005, 2006) were not successful, thereby preventing the extrapolation of the results to more

realistic values of the slip length. It is shown in §3.5, however, that the oscillatory regime at a smaller value of the slip length could still be observed by setting the value of Oh sufficiently low. The good agreement between the results of the DI method and the LS method with a slip condition show that the results presented here are not sensitive to the manner in which the contact-line singularity is alleviated.

The authors would like to thank Lawrence Lau for assistance with implementation of the axisymmetric LS method, and EPSRC for financial support (grant EP/D031222).

REFERENCES

- BIANCE, A.-L., CLANET, C. & QUERÉ, D. 2004 First steps in the spreading of a liquid droplet. *Phys. Rev. E* **69**, 016301.
- COX, R. G. 1998 Inertial and viscous effects on dynamic contact angles. *J. Fluid Mech.* **357**, 249–278.
- DUSSAN, V., E. B. 1979 On the spreading of liquids on solid surfaces: static and dynamic contact lines. *Annu. Rev. Fluid Mech.* **11**, 371–400.
- EGGERS, J. & STONE, H. A. 2004 Characteristic lengths at moving contact lines for a perfectly wetting fluid: the influence of speed on the dynamic contact angle. *J. Fluid Mech.* **505**, 309–321.
- DE GENNES, P. G. Wetting: statics and dynamics. *Rev. Mod. Phys.* **57**, 827.
- HOCKING, L. M. 1983 The spreading of a thin drop by gravity and capillarity. *Q. J. Mech. Appl. Maths* **36**, 55–69.
- HOCKING, L. M. & DAVIS, S. H. 2002 Inertial effects in time-dependent motion of thin films. *J. Fluid Mech.* **467**, 1–17.
- HUH, C. & SCRIVEN, L. E. 1971 Hydrodynamic model of steady movement of a solid/liquid/fluid contact line. *J. Colloid Interface Sci.* **35**, 85–101.
- JACQMIN, D. 1999 Calculation of two-phase Navier-Stokes flows using phase-field modelling. *J. Comput. Phys.* **155**, 96–127.
- JACQMIN, D. 2000 Contact-line dynamics of a diffuse fluid interface. *J. Fluid Mech.* **402**, 57–88.
- MARSH, J. A., GAROFF, S. & DUSSAN, V., E. B. 1993 Dynamic contact angles and hydrodynamics near a moving contact line. *Phys. Rev. Lett.* **70**, 2778–2781.
- RENARDY, M., RENARDY, Y. & LI, J. 2001 Numerical simulation of moving contact line problems using a volume-of-fluid method. *J. Comput. Phys.* **171**, 243–263.
- SHIKHMURZAEV, Y. D. 1997 Moving contact lines in liquid/liquid/solid systems. *J. Fluid Mech.* **334**, 211–249.
- SPELT, P. D. M. 2005 A level-set approach for simulations of flows with multiple moving contact lines with hysteresis. *J. Comput. Phys.* **207**, 389–404.
- SPELT, P. D. M. 2006 Shear flow past two-dimensional droplets pinned or moving on an adhering channel wall at moderate Reynolds numbers: a numerical study. *J. Fluid Mech.* **561**, 439–463.
- STOEVE, K., RAMÉ, E. & GAROFF, S. 1999 Effects of inertia on the hydrodynamics near moving contact lines. *Phys. Fluids* **11**, 3209–3216.
- TANNER, L. H. 1979 The spreading of silicone oil drops on horizontal surfaces. *J. Phys. D* **12**, 1473–1483.
- VILLANUEVA, W. & AMBERG, G. 2006 Some generic capillary-driven flows. *Intl J. Multiphase Flow* **32**, 1072–1086.
- YARIN, A. L. 2006 Droplet impact dynamics: splashing, spreading, receding, bouncing.... *Annu. Rev. Fluid Mech.* **38**, 159–192.